Inorg. Chem. **2004**, *43*, 7187−7195

Oxidation of Mixed-Valence Co^{III}/Fe^{II} Complexes Reversed at High pH: A Kinetico-Mechanistic Study of Water Oxidation

Paul V. Bernhardt,[†] Fernando Bozoglian,[‡] Brendan P. Macpherson,[†] Manuel Martínez,*[,‡] André E. Merbach,[§] Gabriel González,[‡,⊥] and Beatriz Sienra[||]

Department of Chemistry, University of Queensland, Brisbane 4072, Australia, Departament de Química Inorgànica, Universitat de Barcelona, Martí i Franquès 1-11, E-08028 Barcelona, Spain, Institut de Chimie Moléculaire et Biologique, École Polytechnique Fédérale de Lausanne, EPFL-BCH, CH-1015 Lausanne, Switzerland, and Cátedra de Química Inorgánica, Facultad de Química, Universidad de la República, Avenida General Flores 2124, 11800 Montevideo, Uruguay

Received May 26, 2004

The outer-sphere oxidation of Fe^{II} in the mixed-valence complex *trans*-$[L^{14S}Co^{III}NCFe^{II}(CN)_6]^-$, being L^{14S} an N_3S_2 macrocylic donor set on the cobalt(III) center, has been studied. The comparison with the known processes of N_5 macrocycle complexes has been carried out in view of the important differences occurring on the redox potential of the cobalt center. The results indicate that the outer-sphere oxidation reactions with $S_2O_8^{2-}$ and $[Co(ox)_3]^{3-}$ involve a great amount of solvent-assisted hydrogen bonding that, as a consequence from the change from two amines to sulfur donors, are more restricted. This is shown by the more positive values found for $\Delta S^{\ddagger}$ and $\Delta V^{\ddagger}$. The X-ray structure of the oxidized complex has been determined, and it is clearly indicative of the above-mentioned solvent-assisted hydrogen bonding between nitrogen and cyanide donors on the cobalt and iron centers, respectively. *trans*-$[L^{14S}Co^{III}NCFe^{III}(CN)_6]$, as well as the analogous N_5 systems *trans*-$[L^{14}Co^{III}NCFe^{III}(CN)_6]$, *trans*-$[L^{15}Co^{III}NCFe^{III}$-$(CN)_6]$, and *cis*-$[L^{13}Co^{III}NCFe^{III}(CN)_6]$, oxidize water to hydrogen peroxide at pH > 10 with a rather simple stoichiometry, i.e., $[L^nCo^{III}NCFe^{III}(CN)_5] + OH^- \rightarrow [L^nCo^{III}NCFe^{II}(CN)_5]^- + {}^1/_2H_2O_2$. In this way, the reversibility of the iron oxidation process is achieved. The determination of kinetic and thermal and pressure activation parameters for this water to hydrogen peroxide oxidation leads to the kinetic determination of a cyanide based OH^- adduct of the complex. A second-order dependence on the base concentration is associated with deprotonation of this adduct to produce the final inner-sphere reduction process. The activation enthalpies are found to be extremely low (15 to 35 kJ mol^{-1}) and responsible for the very fast reaction observed. The values of $\Delta S^{\ddagger}$ and $\Delta V^{\ddagger}$ (−76 to −113 J K^{-1} mol^{-1} and −5.5 to −8.9 cm^3 mol^{-1}, respectively) indicate a highly organized but not very compressed transition state in agreement with the inner-sphere one-electron transfer from O^{2-} to Fe^{III}.

Introduction

Mixed-valence coordination complexes continue to attract considerable attention. The possible application of such complexes in a wide variety of processes emerges from their valence localization/delocalization character and the properties derived from their intervalence electronic transitions,[1] which are of relevance to magnetism[2,3] and electrochromism.[4] Theoretical studies[5] of the properties directly related to the nature of the metal-to-metal charge transfer (MMCT) energy and its tunability according to solvent, ionic medium, temperature, and pressure variations are many, and they have

* Author to whom correspondence should be addressed. E-mail: manel.martinez@qi.ub.es.
[†] University of Queensland.
[‡] Universitat de Barcelona.
[§] École Polytechnique Fédérale de Lausanne.
[||] Universidad de la República.
[⊥] Present address: Institut Català d'Investigació Química, Avinguda dels Països Catalans s/n, E-43007 Tarragona, Spain.

(1) Robin, M. B.; Day, P. *Adv. Inorg. Chem. Radiochem.* **1967**, *10*, 247−422.
(2) Lescouezec, R.; Vaissermann, J.; Ruiz-Pérez, C.; Lloret, F.; Carrasco, R.; Julve, M.; Verdager, M.; Dromzee, Y.; Gatteschi, D.; Wernsdorfer, W. *Angew. Chem., Int. Ed.* **2003**, *42*, 1483−1486.
(3) Toma, L. M.; Lescouezec, R.; Lloret, F.; Julve, M.; Vaissermann, J.; Verdager, M. *Chem. Commun.* **2003**, 1850−1851.
(4) Rosseinsky, D. R.; Mortimer, R. J. *Adv. Mater.* **2001**, *13*, 783−793.
(5) Hush, N. S. *Prog. Inorg. Chem.* **1967**, *8*, 391−444.

10.1021/ic0493191 CCC: $27.50
Published on Web 10/02/2004

Chart 1

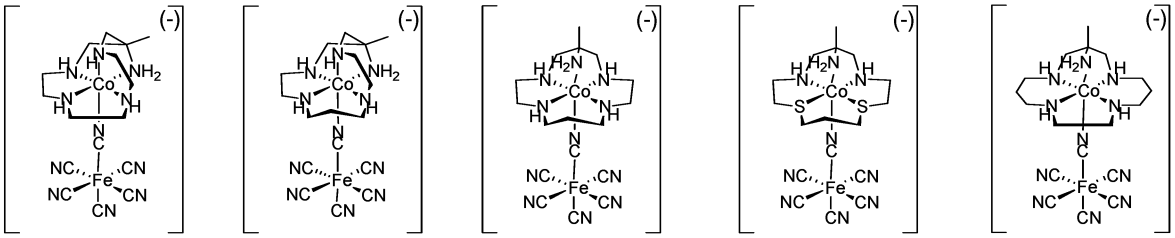

cis-$[L^{13}Co^{III}NCFe^{II}(CN)_5]^-$ *cis*-$[L^{14}Co^{III}NCFe^{II}(CN)_5]^-$ *trans*-$[L^{14}Co^{III}NCFe^{II}(CN)_5]^-$ *trans*-$[L^{14S}Co^{III}NCFe^{II}(CN)_5]^-$ *trans*-$[L^{15}Co^{III}NCFe^{II}(CN)_5]^-$

provided a better understanding of the electronic properties of such species.[6,7] The redox processes that involve the appearance and disappearance of these MMCT bands in the visible or near-IR zone of the electromagnetic spectrum have also been studied in order to clarify the properties and possible uses of the complexes.[4,8,9] Nevertheless, one of the important drawbacks in this field has been the relative scarcity of well-characterized (molecular) mixed-valence compounds where tunability of the MMCT has been possible through modest variations in the structure of the complex.

In recent years we have been involved in the preparation and characterization of a series of mixed-valence cyano-bridged Co^{III}/Fe^{II} dinuclear complexes where the cobalt is coordinated to a variety of pentadentate macrocyclic N_5 ligands (L^n, where *n* indicates the ring size), $[L^nCo^{III}NCFe^{II}(CN)_5]^-$ (Chart 1).[10−12] By doing so, important differences in MMCT bands have been obtained, and the effects of varying temperature, pressure, and ionic strength have been studied.[13,14] Their outer-sphere oxidation reactions ($Co^{III}/Fe^{II} \rightarrow Co^{III}/Fe^{III}$) have also been described, and the results are a clear indication of the importance of hydrogen bonding in these processes as established previously.[15] These interactions involving the macrocyclic amine protons and their geometrical distribution within the complex have been clearly established via the joint determination of entropies and volumes of activation for the oxidations of the nonprotonated and doubly protonated species ($[L^nCo^{III}NCFe^{II}(CN)_5]^-$/$[L^nCo^{III}NCFe^{II}(CN)_3(CNH)_2]^+$) existing in acid−base equilibrium. The values of the corresponding $[L^nCo^{III}NCFe^{II}(CN)_3(CNH)_2]^+ \rightleftarrows [L^nCo^{III}NCFe^{II}(CN)_5]^- + 2H^+$ equilibrium constants, pK_{12}, have also been established.[15]

The preparation of the equivalent species *trans*-$[L^{14S}Co^{III}NCFe^{II}(CN)_5]^-$, where the cobalt-bound macrocycle has been changed from an N_5 to an N_3S_2 set of donors (Chart 1) via a mechanistically directed preparative procedure, has been described elsewhere.[16] The electrochemical data obtained are a clear indication of the softer nature of the mixed donor macrocyclic ligand which produces important changes in the MMCT energy as well as in its outer-sphere redox behavior. In this paper we present the study of its outer-sphere oxidation process by $S_2O_8^{2-}$ and $[Co(ox)_3]^{3-}$ (ox = $C_2O_4^{2-}$) at variable temperature and pressure, and the results are compared with those for the known N_5 systems. The results are interpreted in a similar way to those previously described for the analogous N_5 set of donors on the macrocycle. While second-order kinetics are obtained for peroxodisulfate as oxidizing agent, a limiting kinetic behavior is obtained for the reaction with the higher charged and strong hydrogen acceptor, $[Co(ox)_3]^{3-}$.[17] The kinetic and temperature- and pressure-dependent activation parameters are interpreted in view of the poorer capability of the N_3S_2 macrocycle to donate hydrogen bonds to the oxidizing agent. The X-ray crystal structure of the oxidized form *trans*-$[L^{14S}Co^{III}NCFe^{III}(CN)_5]$ has also been determined, allowing the full characterization of this complex system.

In the course of this oxidation study, the process has been found to behave in a reversible way at high pH values, indicating that the oxidized form of the complex *trans*-$[L^{14S}Co^{III}NCFe^{III}(CN)_5]$ is an effective oxidant of water at pH > 10. The process produces hydrogen peroxide rather than oxygen, an unsual process that has not been previously unambiguously reported. The reaction sequence involves the formation of an OH^- adduct in a rapid pre-equilibrium that further reacts with more base deprotonating and generating the final O_2H^- species after the Fe^{III} to Fe^{II} reduction has taken place. This process has also been studied at variable temperature and pressure, and the reduction reaction of the related *cis*-$[L^{13}Co^{III}NCFe^{III}(CN)_5]$, *trans*-$[L^{14}Co^{III}NCFe^{III}(CN)_5]$, and *trans*-$[L^{15}Co^{III}NCFe^{III}(CN)_5]$ species have also been carried out. The results are interpreted from the point of view of an inner-sphere redox process, similar to related reactions with $[Fe(CN)_6]^{2-/3-}$ systems.[18] The increased acidity of the OH^- coordinated in the adduct[19] accounts for a second-

(6) Haim, A. *Comments Inorg. Chem.* **1985**, *4*, 113−149.
(7) Khoshtariya, D. E.; Bajaj, H. C.; Tregloan, P.; van Eldik, R. *J. Phys. Chem. A* **2000**, *104*, 5535−5544.
(8) Almaraz, A. E.; Gentil, L. A.; Baraldo, L. M.; Olabe, J. A. *Inorg. Chem.* **1996**, *35*, 7718−7727.
(9) Parise, A. R.; Baraldo, L. M.; Olabe, J. A. *Inorg. Chem.* **1996**, *35*, 5080−5086.
(10) Bernhardt, P. V.; Macpherson, B. P.; Martínez, M. *Inorg. Chem.* **2000**, *39*, 5203−5208.
(11) Bernhardt, P. V.; Macpherson, B. P.; Martínez, M. *J. Chem. Soc., Dalton Trans.* **2002**, 1435−1441.
(12) Bernhardt, P. V.; Martinez, M. *Inorg. Chem.* **1999**, *38*, 424−425.
(13) Alzouibi, B. M.; Bernhardt, P. V.; Macpherson, B. P.; Martínez, M.; Tregloan, P.; van Eldik, R. Unpublished results.
(14) López-Pérez, G.; Prado-Gotor, R.; Sánchez, F.; López-López, M.; González-Arjona, D.; Pérez-Tejeda, P.; Bozoglián, F.; González, G.; Martínez, M. Submitted.
(15) Bernhardt, P. V.; Bozoglián, F.; Macpherson, B. P.; Martínez, M.; González, G.; Sienra, B. *Eur. J. Inorg. Chem.* **2003**, 2512−2518.
(16) Bernhardt, P. V.; Bozoglián, F.; Macpherson, B. P.; Martínez, M. *Dalton Trans.* **2004**, 2582−2587.
(17) Warren, R. M. L.; Lappin, A. G.; Tatehata, A. *Inorg. Chem.* **1992**, *31*, 1566−1574.
(18) Murray, R. S. *J. Chem. Soc., Dalton Trans.* **1974**, 2381−2383.

order dependence of the value of the rate on [OH^-] and explains the trends observed.

Experimental Section

Synthesis. *cis*-[$CoL^{14S}Cl]Cl_2$, Na{*cis*-[$L^{13}Co^{III}NCFe^{II}(CN)_5$]}, *trans*-[$L^{15}Co^{III}NCFe^{III}(CN)_5]\cdot 5H_2O$, *trans*-[$L^{14}Co^{III}NCFe^{III}(CN)_5]\cdot 4H_2O$, and Na{*trans*-[$L^{14S}Co^{III}NCFe^{II}(CN)_5$]}$\cdot 7H_2O$ were prepared according to previously described methods.[10,15,16,20] Other chemicals were analytical grade, commercially available, and used without further purification.

[$L^nCo^{III}NCFe^{III}(CN)_5$] ($L^n = L^{13}, L^{14S}$). The general procedure for these new complexes is the same. To a solution of the corresponding Na[$L^nCo^{III}NCFe^{II}(CN)_5$] complex (0.25 g, 0.2×10^{-3} mol) in 25 mL of water, 0.14 g (0.59×10^{-3} mol) of sodium peroxodisulfate was added. The reaction mixture changed from red to yellow within 2 h and was left to crystallize; the yellow crystals obtained were washed with cold water and air-dried.

trans-[$L^{14S}Co^{III}NCFe^{III}(CN)_5]\cdot 4H_2O$. Anal. Calcd (Found) for $C_{17}N_9S_2\,H_{25}CoFe\cdot 4H_2O$: N 20.79 (20.76), C 33.67 (33.47), S 10.57 (10.62), H 5.49 (5.13). IR (KBr disk), $\bar{\nu}/cm^{-1}$: 2107, 2117 (equatorial CN), 2129 (axial CN), 2169 (μ-CN). UV−vis (H_2O) (λ, $\epsilon)_{max}$/(nm, $M^{-1}\,cm^{-1}$): 285, 15100; 411, 900; 438, 900. Cyclic voltamogram $E_{1/2}$/mV (NHE reference): −320, 650 (1.0 M $LiClO_4$). X-ray quality crystals of *trans*-[$L^{14S}Co^{III}NCFe^{III}(CN)_5]\cdot 2H_2O$ were obtained by slow recrystallization in water in a cool cabinet.

cis-[$L^{13}Co^{III}NCFe^{III}(CN)_5]\cdot 5H_2O$. Anal. Calcd(Found) for $C_{16}N_{21}H_{25}\,O_5CoFe\cdot 5H_2O$: N 26.73 (26,77), C 33.35 (33.24), H 6.12 (6.06). IR (KBr disk), $\bar{\nu}/cm^{-1}$: 2111 (equatorial CN), 2120 (axial CN), 2171 (μ-CN). UV−vis (H_2O) (λ, $\epsilon)_{max}$/(nm, $M^{-1}\,cm^{-1}$): 328, 1063; 408, 869; 437, 950. Cyclic voltamogram $E_{1/2}$/mV (NHE reference): −543, 626 (1.0 M $LiClO_4$).

Protonation Constants. Spectrophotometric titrations[21] (1.0 M $HClO_4$) of the mixed-valence *trans*-[$L^{14S}Co^{III}NCFe^{II}(CN)_5$] complex were carried out on a Cary 50 instrument to determine its acidity constants. Solutions were transferred to a 50 mL cell and thermostated at 25 °C; addition of small amounts of standard 0.1 M NaOH produced successive changes in the UV−vis spectrum with pH which indicated the presence of two distinct processes as found for the equivalent N_5 systems.[15] As before, the pK_a values determined by the use of the SPECFIT software[22] were too close to allow the selective formation of the monoprotonated complex. Consequently only pβ_{12} could be determined, and hence studies on the nonprotonated and diprotonated species were carried out.

Electrochemistry. Electrochemical experiments were carried out with a EG&G PAR 263A instrument with a platinum wire working electrode, a platinum wire secondary electrode, and a Ag/AgCl reference electrode; solutions were degassed prior to the cyclic voltammetry experiment. Voltammograms of the complexes were carried out at 1×10^{-3} M complex concentration in 1.0 M $LiClO_4$.

Crystallography. Cell constants were determined by a least-squares fit to the setting parameters of 25 independent reflections measured on an Enraf-Nonius CAD4 four-circle diffractometer employing graphite monochromated Mo Kα radiation (0.71073 Å) and operating in the $\omega-2\theta$ scan mode. Data reduction and empirical absorption corrections (Ψ-scans) were performed with the WINGX[23] package. The structure was solved by Paterson methods with SHELXS-86 and refined by full-matrix least-squares analysis with SHELXL-97.[24] The H atoms of the two water molecules were located from difference maps and then restrained to their parent O-atom using a riding model. The drawing of the complex (Figure 1) was produced with ORTEP3.[25] All non-hydrogen atoms were modeled with anisotropic thermal parameters. Table 1 collects the relevant crystallographic data.

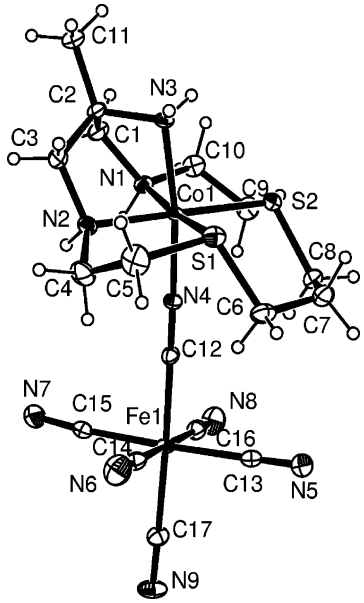

Figure 1. *trans*-[$L^{14S}Co^{III}NCFe^{III}(CN)_5$]. Selected bond lengths (Å) and angles (deg): Co(1)−N(1) 1.971(3); Co(1)−N(2) 1.963(2); Co(1)−N(3) 1.943(2); Co(1)−N(4) 1.887(2); Co(1)−S(1) 2.2167(9); Co(1)−S(2) 2.2188(8); Fe(1)−C(12) 1.916(3); Fe(1)−C(13−17) 1.939(3)−1.950(3); Co(1)−N(4)−C(12) 174.3(3); Fe(1)−C−N 174.9(3)−179.9(4).

Table 1. Crystal Data

formula	$C_{17}H_{29}CoFeN_9O_2S_2$	Z	4
fw	570.39	T/K	296(2)
space group	$P\,2_1/n$ (No. 14, variant on $P\,2_1/c$)	λ/Å	0.71073
a/Å	11.6307(7)	μ/cm^{-1}	14.48
b/Å	14.659(1)	D_c/g cm^{-3}	1.521
c/Å	14.613(1)	$R(F_o)^a$	0.0335
β/deg	90.763(5)	$R_w(F_o^2)^b$	0.0889
V/Å^3	2491.2(3)		

^{a} $R(F_o) = \sum||F_o| - |F_c||/\sum|F_o|$. ^{b} $R_w(F_o^2) = [\sum w(F_o^2 - F_c^2)/\sum wF_o^2]^{1/2}$.

Kinetic Measurements. Reactions were followed by UV−vis spectroscopy in the full 800−300 nm range. Observed rate constants were derived from the absorbance vs time traces at wavelengths where a maximum increase or decrease of absorbance was observed. No dependence of the observed rate constant values on the selected wavelengths was detected, as expected for reactions where a good retention of isosbestic points is observed. The general kinetic technique is that previously described.[15,26] In all cases pseudo-first-order conditions were maintained, and the complex concentration was kept at $(2-5) \times 10^{-4}$ M. Neither the oxidation nor the reduction rate constants showed any trend on the concentration of the metal species, which is indicative of a simple stoichiometry for the reactions studied. At atmospheric pressure, runs with $t_{1/2} > 170$ s

(19) Wilkins, R. G. *Kinetics and Mechanisms of Reactions of Transition Metal Complexes*; VCH: Weinheim, 1991.
(20) Lawrance, G. A.; Martínez, M.; Skelton, B. W.; White, A. H. *Aust. J. Chem.* **1991**, *44*, 113−121.
(21) Perkampus, H. H. *UV−Vis Spectroscopy and Its Applications*; Springer: Berlin, 1992.
(22) Binstead, R. A.; Zuberbühler, A.; Jung, B. *SPECFIT* [3.0.34], 2003.
(23) Farrugia, L. J. *J. Appl. Crystallogr.* **1999**, *32*, 837−838.
(24) Sheldrick, G. M. *SHELX-97: Programs for Crystal Structure Analysis* [Release 97-2], Institut für Anorganishe Chemie, Universität Göttingen: Germany, 1998.
(25) Farrugia, L. J. *J. Appl. Crystallogr.* **1997**, *30*, 565.
(26) Martínez, M.; Pitarque, M.; van Eldik, R. *Inorg. Chim. Acta* **1997**, *256*, 51−59.

were recorded on an HP8452A instrument equipped with a thermostated multicell transport while for runs with $t_{1/2} < 7$ s an Applied-Photophysics stopped-flow instrument connected to a J&M TIDAS spectrophotometer was used. For runs at variable pressure, temperature, and concentration, conditions were set in a way that all kinetic measurements could be carried out by the use of a homemade stopped-flow instrument connected to a J&M TIDAS spectrophotometer.[27] All the values obtained for the pseudo-first-order rate constants as a function of dinuclear metal complex, temperature, pressure, and [OH^-] are collected in Tables S1 and S2.

Hydrogen Peroxide and Oxygen Detection. The hydrogen peroxide formed during the reaction was measured by the standard method which uses Mohr salt as reductant, the iron(III) formed being complexed by xylenol orange; the absorbance at 590 nm of the complex allows the evaluation of the hydrogen peroxide concentration.[28,29] Solutions were degassed prior to the measurements. Blank experiments performed on solutions of the Co^{III}/Fe^{II} species indicated that no H_2O_2 is produced from the reaction medium. Free oxygen concentrations were determined with a CRISON oxymeter OXI330 detector with a sensor cell OX305.

Results

Compounds. The crystal structure of *trans*-[$L^{14S}Co^{III}$-$NCFe^{III}(CN)_5$]·$2H_2O$ was determined, and a view of the complex is shown in Figure 1. The trans coordination mode of the macrocycle is apparent with the pendent primary amine coordinating in the axial site orthogonal to the macrocyclic plane. The configuration of the macrocyclic donors may be described as *trans*-III, where the two amine H-atoms point down (as drawn) and the S-donor lone pairs point up. The conformation of the two five-membered chelate rings is identical resulting in a staggered orientation. The conformation of the ligand is identical to that defined in the crystal structure of the one-electron-reduced parent Na{*trans*-[L^{14S}-$Co^{III}NCFe^{II}(CN)_5$]}·$5^1/_2H_2O$·$^1/_2$EtOH.[16]

There are some notable bond length variations between *trans*-[$L^{14S}Co^{III}NCFe^{III}(CN)_5$]·$2H_2O$ and *trans*-[$L^{14}Co^{III}$-$NCFe^{III}(CN)_5$]·$5H_2O$, the pentaamine analogue.[11] Although the corresponding $Co-N_{amine}$ bond lengths in the two structures are the same within experimental error, the Co−N≡C coordinate bond is significantly shorter in *trans*-[L^{14S}-$Co^{III}NCFe^{III}(CN)_5$] (1.887(2) Å) compared with *trans*-[L^{14}-$Co^{III}NCFe^{III}(CN)_5$] (1.913(4) Å). Also, the Fe(1)−C(12) bond length (1.916(3) Å) to the bridging ligand is much shorter than those to the remaining terminal cyano ligands (1.94−5 Å), whereas no significant variation in the six Fe−C≡N coordinate bonds was seen for *trans*-[$L^{14}Co^{III}NCFe^{III}(CN)_5$].

The *trans*-[$L^{14}Co^{III}NCFe^{III}(CN)_5$] complex exhibits a *trans*-I configuration of the four secondary amines, where all four amine protons point toward the ferricyanide group. These protons repel the ferrocyanide group somewhat and may lengthen the Co−N and Fe−C coordinate bonds relative to that seen for *trans*-[$L^{14S}Co^{III}NCFe^{III}(CN)_5$], where two of these protons are absent. However, the fact remains that the Fe(1)−C(12) bond length is significantly shortened by comparison with the terminal Fe−C≡N coordinate bonds and those found in the uncomplexed ferricyanide anion.[30] The origin of this unusual observation is not obvious, but an electronic influence exerted by the two π-acceptor S-donors via the Co center is the most likely cause, which strengthens both coordinate bonds associated with the bridging cyano ligand. There is no significant effect on the C≡N bond length of the bridging ligand, which is comparable with those of the terminal ligands.

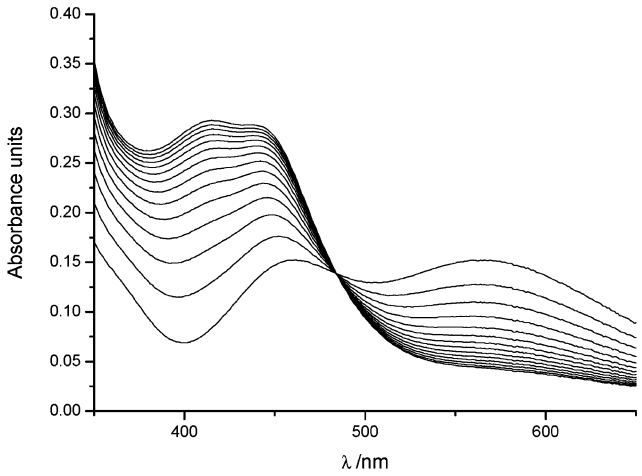

Figure 2. UV−vis spectral changes obtained for the oxidation reaction of complex *trans*-[$L^{14S}Co^{III}NCFe^{II}(CN)_5]^-$ with $S_2O_8^{2-}$ ($T = 20$ °C, pH = 5.0, $I = 1.0$ M $LiClO_4$, [complex] = 5×10^{-4} M, [$S_2O_8^{2-}$] = 10×10^{-3} M).

The structure comprises a network of dinuclear complexes linked by intermolecular H-bonds. The two water molecules in the asymmetric unit make strong bridging H-bonds between terminal cyano N-atoms on different complexes: O(1)−H(1C)···N(7), 2.17 Å, 179°; O(1D)−H(1D)···N(5)′, 1.93 Å, 169° (symmetry code $-x + {}^5/_2$, $y + {}^1/_2$, $-z + {}^1/_2$); O(2)−H(2C)···N(6)″, 1.93 Å, 162° (symmetry code $x - {}^1/_2$, $-y + {}^1/_2$, $z + {}^1/_2$); O(2)−H(2D)···N8‴, 1.90 Å, 158° (symmetry code $x - 1$, y, z). The most significant H-bonding interactions involving the coordinated amines are with the water molecules (N(2)−H(2)···O(1), 1.94 Å, 174° and N(3)−H(3D)···O(2), 2.02 Å, 160°) and a terminal cyano N-atom (N(3)−H(3C)···N(9)′, 2.19 Å, 161° (symmetry code $x - 1$, y, z)).

Mixed-Valence Co^{III}/Fe^{II} Complex Oxidation Kinetics. In view of the very different redox and spectral properties of the complex anion *trans*-[$L^{14S}Co^{III}NCFe^{II}(CN)_5]^-$ ($E°_{Co^{III}/Co^{II}} = -560$ mV; $E°_{Fe^{III}/Fe^{II}} = 650$ mV; MMCT 438 nm, 900 M^{-1} cm^{-1}) by comparison with its pentaamine analogue *trans*-[$L^{14}Co^{III}NCFe^{II}(CN)_5]^-$ ($E°_{Co^{III}/Co^{II}} = -320$ mV; $E°_{Fe^{III}/Fe^{II}} = 644$ mV; MMCT 513 nm, 490 M^{-1} cm^{-1}),[16] the study of its redox behavior with typical outer-sphere oxidants such as $S_2O_8^{2-}$ and $[Co(ox)_3]^{3-}$ was pursued (Figure 2). The studies were carried out taking into account the value of $p\beta_{12} = 2.6$, which accounts for the *trans*-[$L^{14S}Co^{III}NCFe^{II}(CN)_5]^-$/*trans*-[$L^{14S}Co^{III}NCFe^{II}(CN)_3(CNH)_2]^+$ species distribution. In

(27) Bugnon, P.; Laurency, G.; Ducommun, Y.; Sauvegeat, P.; Merbach, A. E. *Anal. Chem.* **1996**, *68*, 3045−3049.
(28) Jiang, Z. Y.; Woollard, A. C. S.; Wolff, S. P. *Lipids* **1991**, *26*, 853−586.
(29) Nourooz-Zadeh, J.; Tajaddini-Sarmadi, J.; Wolff, S. P. *Anal. Biochem.* **1994**, *220*, 406−409.
(30) Marsh, R. E. *Acta Crystallogr.* **1995**, *B51*, 897−907.

Table 2. Kinetic, Thermal, and Baric Activation Parameters for the Oxidation Processes of Complex *trans*-$[L^{14S}Co^{III}NCFe^{II}(CN)_5]^-$ with Different Oxidants and at Different Acidities (I = 1.0 M $LiClO_4$)

species	oxidant	$k^{298} \times 10^2/M^{-1}\ s^{-1}$	$\Delta H^{\ddagger}$/kJ mol^{-1}	$\Delta S^{\ddagger}$/J K^{-1} mol^{-1}	$\Delta V^{\ddagger}$ /cm^3 mol^{-1} (T /K)
trans-$[L^{14S}Co^{III}NCFe^{II}(CN)_5]^-$	$S_2O_8^{2-}$	7.4	73 ± 2	−23 ± 6	8.1 ± 0.5 (291)
trans-$[L^{14S}Co^{III}NCFe^{II}(CN)_3(CNH)_2]^+$	$S_2O_8^{2-}$	18	91 ± 2	44 ± 7	not determined
trans-$[L^{14S}Co^{III}NCFe^{II}(CN)_5]^-$	$[Co(ox)_3]^{3-}$	0.056[b]	81 ± 6	−37 ± 19	13 ± 1 (293)
trans-$[L^{14}Co^{III}NCFe^{II}(CN)_5]^-$ [a]	$S_2O_8^{2-}$	5.0	61 ± 1	−65 ± 3	4.1 ± 0.1
trans-$[L^{14}Co^{III}NCFe^{II}(CN)_3(CNH)_2]^+$	$S_2O_8^{2-}$	5.6	80 ± 2	2 ± 7	1.5 ± 0.1
trans-$[L^{14}Co^{III}NCFe^{II}(CN)_5]^-$ [a]	$[Co(ox)_3]^{3-}$	0.10[c]	51 ± 2	−131 ± 8	12 ± 1
trans-$[L^{15}Co^{III}NCFe^{II}(CN)_5]^-$ [a]	$S_2O_8^{2-}$	16	55 ± 5	−76 ± 16	19 ± 2
trans-$[L^{15}Co^{III}NCFe^{II}(CN)_3(CNH)_2]^+$	$S_2O_8^{2-}$	18	85 ± 4	23 ± 15	11 ± 1
trans-$[L^{15}Co^{III}NCFe^{II}(CN)_5]^-$ [a]	$[Co(ox)_3]^{3-}$	0.11[c]	63 ± 6	−90 ± 19	18 ± 2

[a] Relevant data for the oxidation of *trans*-$[L^{14}Co^{III}NCFe^{II}(CN)_5]^-$ and *trans*-$[L^{15}Co^{III}NCFe^{II}(CN)_5]^-$ from ref 15 have been included for comparison purposes. [b] In s^{-1}, K_{OS} = 120 M^{-1}. [c] In s^{-1}.

this way, comparison of the data with those available for the related dinuclear mixed-valence complexes, where the cobalt moiety is coordinated by different sized N_5 macrocycles is possible.[15] For the $S_2O_8^{2-}$ oxidation process, second-order behavior is observed,[31] while for $[Co(ox)_3]^{3-}$ a limiting kinetic scheme applies (Figure S1).[32]

The reaction scheme and rate law derived for the two processes are the same as those applied in previous studies, and the value of $p\beta_{12}$ is very similar to that determined for the related complexes with different sized N_5 macrocycles.[15] Table 2 collects all the kinetic and activation parameters determined in this study together with the relevant values of the analogous systems that have been studied previously. The values obtained for the kinetic and, both thermal and pressure, activation parameters show the same general trends in the entropies and volumes of activation as those obtained for the previously studied systems. Nevertheless, the absolute values of $\Delta H^{\ddagger}$, $\Delta S^{\ddagger}$, and $\Delta V^{\ddagger}$ for the oxidation with trisoxalatocobaltate(III) of the nonprotonated complex show important differences (Table 2) when two secondary amines are substituted by sulfur donors.

The processes studied with $S_2O_8^{2-}$ as oxidant were found to produce well-behaved first-order absorbance vs time traces in the pH range where the doubly protonated complex exists as the sole compound. When the pH value was increased for the study of the nonprotonated species, the spectral changes became more erratic; even at pH > 10, no reliable values of k_{obs} could be obtained. Under these conditions, the redox reactions were observed to revert to the original Co^{III}/Fe^{II} reduced form of the complex over long periods, which implied that all the oxidizing agent had been consumed in a catalytic process. This (reverse) reduction reaction becomes dominant when the concentration of peroxodisulfate is low, and no oxidation reaction is observed at pH = 11 with stoichiometric amounts of oxidant. Under these conditions, evolution of oxygen bubbles was observed. Similar observations were not apparent for blank solutions of $Na_2S_2O_8$ and were ascribed to a redox process involving the oxidized Co^{III}/Fe^{III} complex.

Co^{III}/Fe^{III} Complex Reduction Kinetics. In view of the above-mentioned results, the reduction processes of the complexes *cis*-$[L^{13}Co^{III}NCFe^{III}(CN)_5]$, *trans*-$[L^{14}Co^{III}NCFe^{III}(CN)_5]$, *trans*-$[L^{14S}Co^{III}NCFe^{III}(CN)_5]$, and *trans*-$[L^{15}Co^{III}NCFe^{III}(CN)_5]$ were studied. These complexes are stable at neutral pH, but when NaOH is added, the reduced (Co^{III}/Fe^{II}) compound is immediately formed, as shown by the spectral changes indicated in Figure 3. The process is found to be dependent on the value of $[OH^-]$ with a nonlinear dependence as shown in Figure 4.

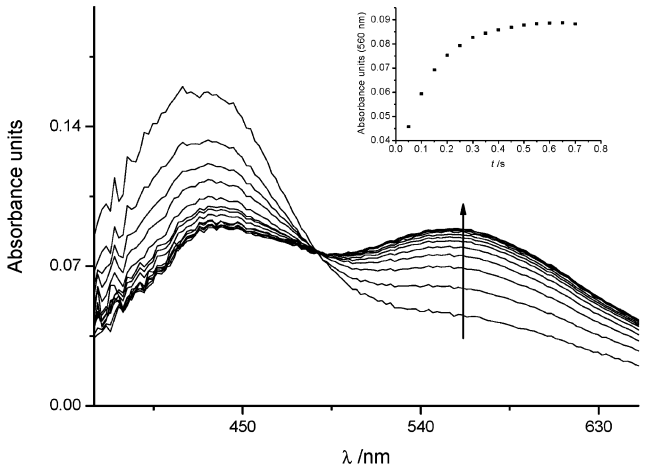

Figure 3. UV−vis spectral changes obtained for OH^- reduction reaction of *trans*-$[L^{14S}Co^{III}NCFe^{III}(CN)_5]$ with NaOH (T = 15 °C, P = 300 atm, I = 1.0 M $LiClO_4$, [complex] = 5 × 10^{-4} M, $[OH^-]$ = 0.040 M).

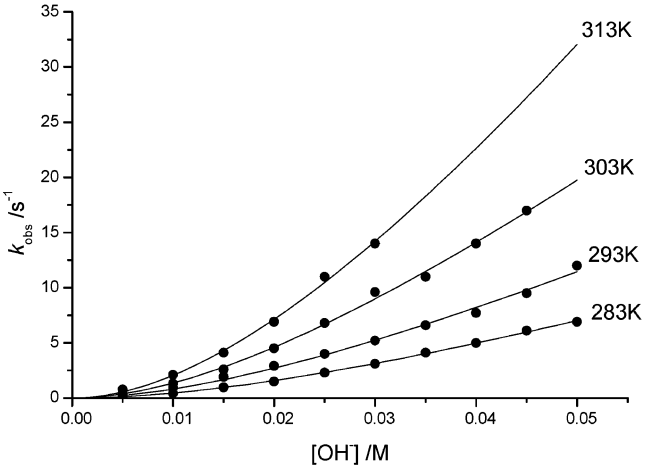

Figure 4. Plot of k_{obs} vs $[OH^-]$ for the reduction of *trans*-$[L^{14S}Co^{III}NCFe^{III}(CN)_5]$ at different temperatures (I = 1.0 M $LiClO_4$).

The base concentration dependence is inconsistent with a rate law of the type $k_{obs} = a[OH^-]^2$ or $k_{obs} = a[OH^-]^2 +$

(31) Fagalde, F.; Katz, N. E.; Povse, V. G.; Olabe, J. A. *Polyhedron* **1998**, *18*, 25−31.
(32) Marusak, R. A.; Osvath, P.; Kemper, M.; Lappin, A. G. *Inorg. Chem.* **1989**, *28*, 1542−1548.

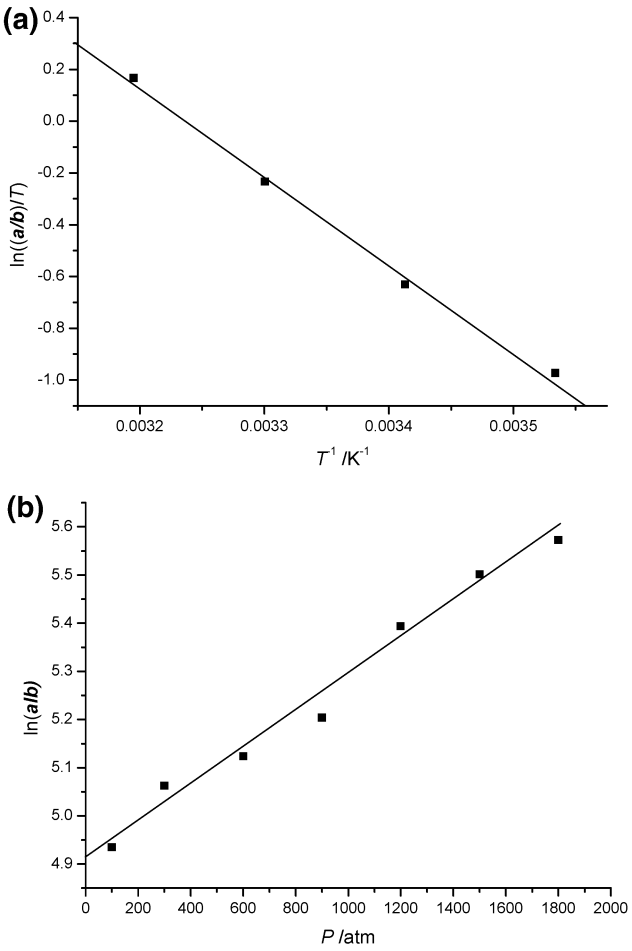

Figure 5. (a) Eyring plot for the parameter (a/b) of the rate law applied to the reduction reaction of *trans*-[$L^{14}Co^{III}NCFe^{III}(CN)_5$] with base ($I$ = 1.0 M $LiClO_4$). (b) ln(a/b) vs P plot for the same process at 15 °C.

b[OH^-] although a simple linear behavior is observed at high base concentration values. The best fit to the data corresponds to a rate law of the type $k_{obs} = (a[OH^-]^2)/(1 + b[OH^-])$; the fit is that shown in Figure 4. While a clear trend of a with temperature and pressure is observed, the values of b have a much larger error and no trend is observed. As seen in the next section, the values of the ratio a/b can be related to a second-order electron-transfer constant, while the term b corresponds to an adduct formation equilibrium constant. In this way the Eyring plots for the a/b term as well as the ln(a/b) vs P plots could be constructed (Figure 5); Table 3 collects all the kinetic, thermal, and pressure activation parameters derived from these plots.

To check the stoichiometry of the reaction, oxygen evolution analysis was carried out on degassed solutions of the oxidized Co^{III}/Fe^{III} dinuclear complexes to which argon-purged NaOH was added. In all cases no oxygen was detected over extended periods as determined by an oxygen-measuring electrode. The measure of H_2O_2 concentration of these reaction mixtures, via spectrophotometric titration using Mohr salt and xylenol orange,[28,29] indicated that hydrogen peroxide is produced in an Fe/H_2O_2 stoichiometric ratio of 1.95; the reaction thus being: $[L^nCo^{III}NCFe^{III}(CN)_5] + OH^- \rightarrow [L^nCo^{III}NCFe^{II}(CN)_5]^- + {}^1/_2H_2O_2$. Consequently, the oxygen bubbles detected must correspond to subsequent decomposition of H_2O_2 formed in the stoichiometric reaction. The absence of any dependence of the rate constants on the concentration of the Co^{III}/Fe^{III} complexes is a clear indicator that the reaction does not involve the operation of two oxidizing metal centers as for some oxygen-producing reactions of the same type.[18,33−37]

Discussion

Complex Oxidation. The reaction scheme and rate law operating for the outer-sphere oxidation process are those indicated in Scheme 1. When the oxidant is $S_2O_8^{2-}$, the observed rate constant shows a linear dependence with the peroxodisulfate concentration. For the oxidation with $[Co(ox)_3]^{3-}$, a limiting first-order behavior is observed, consistent with a redox mechanism involving a kinetically significant outer-sphere precursor complex formation (Figure S1).

The kinetic and activation parameters obtained for the oxidation with $S_2O_8^{2-}$ for the complexes *trans*-[$L^{14S}Co^{III}$-$NCFe^{II}(CN)_5]^-$ and *trans*-[$L^{14S}Co^{III}NCFe^{II}(CN)_3(CNH)_2]^+$ are similar to those measured for previously described systems (Table 2).[15] The activation entropy values (−23 and +44 J K^{-1} mol^{-1}, respectively) indicate the important difference in electrostriction for the formation of the respective outer-sphere complexes. For the anionic *trans*-[$L^{14S}Co^{III}NCFe^{II}$-$(CN)_5]^-$ complex, the charge combination with the anionic oxidant does not reduce the global charge,[8,9,31] while for the cationic diprotonated complex, *trans*-[$L^{14S}Co^{III}NCFe^{II}(CN)_3$-$(CNH)_2]^+$, the charge is reduced on formation of the precursor complex. This results in a much more positive electrostriction entropy value for the latter. As seen in Table 2, these rate enhancements are compensated by an increase in $\Delta H^{\ddagger}$, producing similar $\Delta G^{\ddagger}$ for both species.

When $\Delta S^{\ddagger}$ is compared with $\Delta V^{\ddagger}$ for these systems, no parallel behavior is observed. Taking into account that the intrinsic changes in the {$Fe(CN)_5$} moiety are known to be minimal[38] and that electrostriction should produce the same effects in both parameters, solvent-assisted hydrogen interactions must be responsible for the differences observed.[26,39−42] These interactions explain the expansive ordering observed for the oxidation of *trans*-[$L^{14S}Co^{III}NCFe^{II}(CN)_5]^-$; for *trans*-[$L^{14S}Co^{III}NCFe^{II}(CN)_3(CNH)_2]^+$ the hydrogen bonding ordering effect is compensated by the large electrostriction drop on the precursor formation equilibrium.

For the deprotonated and doubly protonated forms of both 14-membered macrocycle complexes (L^{14} and L^{14S}), the

(33) Bhakare, H. A.; Rao, C. V. N. *J. Indian Chem. Soc* **1974**, *51*, 543−544.
(34) Thusius, D. D.; Taube, H. *J. Am. Chem. Soc.* **1966**, *88*, 850−851.
(35) Anbar, M.; Pecht, I. *J. Am. Chem. Soc.* **1967**, *89*, 2553−2556.
(36) Lancanster, J. M.; Murray, R. S. *J. Chem. Soc. A* **1971**, 2755−2758.
(37) Eaton, D. R.; Pankratz, M. *Can. J. Chem.* **1985**, *63*, 793−797.
(38) Sharpe, A. G. *The Chemistry of Cyano Complexes of the Transition Metals*; Academic Press: London, 1976.
(39) Gallego, C.; González, G.; Martínez, M.; Merbach, A. E. *Organometallics* **2004**, *23*, 2434−2438.
(40) Geselowitz, D. A.; Hammershoi, A.; Taube, H. *Inorg. Chem.* **1987**, *26*, 1842−1845.
(41) Martínez, M.; Pitarque, M.; van Eldik, R. *J. Chem. Soc., Dalton Trans.* **1994**, 3159−3163.
(42) Martínez, M.; Pitarque, M. A. *J. Chem. Soc., Dalton Trans.* **1995**, 4107−4111.

Table 3. Kinetic, Thermal and Baric Activation Parameters for the Water Oxidation Processes by the Complexes $[L^nCo^{III}NCFe^{III}(CN)_5]$ Studied (I = 1.0 M $LiClO_4$)

complex	b^a/M^{-1}	$(a/b)^{298} \times 10^3/M^{-1}\ s^{-1}$	$\Delta H^{\ddagger}$/kJ mol^{-1}	$\Delta S^{\ddagger}$/ J K^{-1} mol^{-1}	$\Delta V^{\ddagger}$/cm^3 mol^{-1}(T/K)
cis-$[L^{13}Co^{III}NCFe^{III}(CN)_5]$	21	2.2	27 ± 1	−91 ± 5	not determined
trans-$[L^{14}Co^{III}NCFe^{III}(CN)_5]$	22	0.20	28 ± 1	−108 ± 4	−8.9 ± 0.5 (288)
trans-$[L^{14S}Co^{III}NCFe^{III}(CN)_5]$	22	0.60	35 ± 3	−76 ± 9	−5.5 ± 0.4 (288)
trans-$[L^{15}Co^{III}NCFe^{III}(CN)_5]$	26	24	15 ± 1	−113 ± 5	−9.6 ± 0.3 (288)

[a] Average for the reaction conditions studied.

Scheme 1

$$trans\text{-}[L^{14S}Co^{III}NCFe^{II}(CN)_5]^- + oxd \overset{K_{OS}}{\rightleftharpoons} \{trans\text{-}[L^{14S}Co^{III}NCFe^{II}(CN)_5]^-;oxd\} \quad (1.1)$$

$$\{trans\text{-}[L^{14S}Co^{III}NCFe^{II}(CN)_5]^-;oxd\} \xrightarrow{k_{et}} \{trans\text{-}[L^{14S}Co^{III}NCFe^{III}(CN)_5]^0;red\} \quad (1.2)$$

$$\{trans\text{-}[L^{14S}Co^{III}NCFe^{III}(CN)_5]^0;red\} \rightleftharpoons trans\text{-}[L^{14S}Co^{III}NCFe^{III}(CN)_5]^0 + red \quad (1.3)$$

$$k_{obs} = \frac{K_{OS}k_{et}[oxd]}{1 + K_{OS}[oxd]} \qquad \text{when oxd is } [Co(ox)_3]^{3-} \quad (1.4)$$

$$k_{obs} = K_{OS}k_{et}[oxd] \qquad \text{when oxd is } S_2O_8^{2-} \quad (1.5)$$

differences between the values of the activation enthalpy and entropy are ca. 20kJ mol^{-1} and 60 J K^{-1} mol^{-1}, respectively. For the L^{15} ligand complexes, these differences are 10 and 40 units lower. It is clear that the size of the ligand plays a very important role in the energetics of the oxidation reaction.[15,43] Furthermore, the change from an N_5 to an N_3S_2 macrocycle (Chart 1) around the Co^{III} center is responsible for a positive shift in $\Delta H^{\ddagger}$ and $\Delta S^{\ddagger}$. The absence of two nitrogens in the N_3S_2 macrocycle is probably the direct cause of such increase, especially if we consider the above-mentioned important contribution of hydrogen bonding interactions in the activation parameters. It may also be pertinent to note that the configuration of the macrocyclic donor atoms changes going from *trans*-$[L^{14}Co^{III}NCFe^{II}(CN)_5]^-$ (*trans*-I, all amine H-atoms pointing toward the $\{Fe(CN)_6\}$ moiety) to *trans*-$[L^{14S}Co^{III}NCFe^{II}(CN)_5]^-$ (*trans*-III, the two amine H-atoms pointing toward the $\{Fe(CN)_6\}$ moiety and the S-donor lone pairs pointing away).

For the oxidation with $[Co(ox)_3]^{3-}$, given the rate law applied, the neat determination of the electron-transfer rate constant can be accomplished (Scheme 1). The value determined for K_{OS} is 120 M^{-1}, very similar to that obtained for the known analogous systems. The thermal activation parameter indicated in Table 2 shows important differences between *trans*-$[L^{14S}Co^{III}NCFe^{II}(CN)_5]^-$ and the previously published *trans*-$[L^{14}Co^{III}NCFe^{II}(CN)_5]^-$ and *trans*-$[L^{15}Co^{III}NCFe^{II}(CN)_5]^-$ complexes although $\Delta V^{\ddagger}$ values are comparable. Since the electrostriction contribution for the proper electron-transfer process is the same for all the systems, the differences observed have to be again related to possible solvent-assisted hydrogen bonding interactions. This is not surprising since the crucial implication of hydrogen bonding interactions in the oxidation reactions by $[Co(ox)_3]^{3-}$ has already been established. Even its involvement in chiral recognition has been studied successfully.[17]

Water Oxidation. While water oxidation by metal complexes has been established for a long time, a complex stoichiometry for the reaction applies in most cases.[35] The evolution of oxygen from the solution is normally associated with the formation of hydroxide bridged species[33] that produces the right electron stoichiometry for the appearance of molecular oxygen.[44] Few reactions that unequivocally produce hydrogen peroxide as the water oxidation product have been fully studied from a kinetico-mechanistic point of view.[34] Any redox process involving the Co^{III} center via deprotonation on the macrocyclic ligand has already been discarded in other work,[45] and the operation of a similar process as the one observed for the present system has already been established for other reactions related with the $\{Fe^{III}(CN)_5\}$ moiety.[18,36,46] In some these cases, the formation of an adduct species with the reducing agent has been established as a prior necessary condition to the Fe^{III} reduction process. Nevertheless, the reaction stoichiometry is not as simple, and two oxidizing metal centers are involved in the full process.[37]

In our case, the stoichiometry is much simpler although the trend indicated in Figure 4 shows a rather complicated involvement of the $[OH^-]$ in the rate law applied. The application of the equation $k_{obs} = (a[OH^-]^2)/(1 + b[OH^-])$ can be easily rationalized by the reaction mechanism indicated in Scheme 2. Term b corresponds directly to the equilibrium constant depicted by K_{add} while term (a/b) is the outer sphere electron-transfer rate constant, k_{et}. In this reaction scheme, the initial equilibrium (2.1) produces an OH^- adduct of the dinuclear complex (similar to those found

(43) González, G.; Martínez, M.; Rodríguez, E. *Eur. J. Inorg.Chem.* **2000**, 1333−1338.
(44) Feig, A. L.; Becker, M.; Schindler, S.; van Eldik, R.; Lippard, S. J. *Inorg. Chem.* **1996**, *35*, 2590−2601.
(45) Hambley, T. W.; Lawrance, G. A.; Martínez, M.; Skelton, B. W.; White, A. W. *J. Chem. Soc., Dalton Trans.* **1992**, 1643−1648.
(46) Schilt, A. *J. Am. Chem. Soc.* **1960**, *82*, 3000−3005.

Scheme 2

$$[L^nCo^{III}NCFe^{III}(CN)_5]^0 + OH^- \underset{}{\overset{K_{add}}{\rightleftharpoons}} \{[L^nCo^{III}NCFe^{III}(CN)_5]\cdot OH\}^- \quad \textbf{(2.1)}$$

$$\{[L^nCo^{III}NCFe^{III}(CN)_5]\cdot OH\}^- + OH^- \xrightarrow{k_{et}} \{[L^nCo^{III}NCFe^{II}(CN)_5]\cdot OH\}^{2-} + \cdot OH \quad \textbf{(2.2)}$$

$$\{[L^nCo^{III}NCFe^{II}(CN)_5]\cdot OH\}^{2-} \xrightarrow{\text{fast}} \{[L^nCo^{III}NCFe^{II}(CN)_5]\}^- + OH^- \quad \textbf{(2.3)}$$

$$\cdot OH + OH^- \underset{}{\overset{K_a}{\rightleftharpoons}} H_2O + O^{\cdot -} \quad \textbf{(2.4)}$$

$$1/2\ O^{\cdot -} + 1/2\ O^{\cdot -} \xrightarrow{\text{fast}} 1/2\ O_2^{2-} \quad \textbf{(2.5)}$$

$$1/2\ O_2^{2-} + H_2O \underset{}{\overset{K_{a'}^{-1}}{\rightleftharpoons}} 1/2\ O_2H^- + OH^- \quad \textbf{(2.6)}$$

$$k_{obs} = \frac{K_{add}k_{et}[OH^-]^2}{1 + K_{add}[OH^-]} \quad \textbf{(2.7)}$$

Scheme 3

$$[L^nCo^{III}NCFe^{III}(CN)_5]^0 + OH^- \underset{}{\overset{K_{add}}{\rightleftharpoons}} \{[L^nCo^{III}NCFe^{III}(CN)_5]\cdot OH\}^- \quad \textbf{(3.1)}$$

$$\{[L^nCo^{III}NCFe^{III}(CN)_5]\cdot OH\}^- + OH^- \underset{}{\overset{K_{dep}}{\rightleftharpoons}} \{[L^nCo^{III}NCFe^{III}(CN)_5]\cdot O\}^{2-} + H_2O \quad \textbf{(3.2)}$$

$$\{[L^nCo^{III}NCFe^{III}(CN)_5]\cdot O\}^{2-} \xrightarrow{k_{et}} \{[L^nCo^{III}NCFe^{II}(CN)_5]\cdot O^{\cdot}\}^{2-} \quad \textbf{(3.3)}$$

$$\{[L^nCo^{III}NCFe^{II}(CN)_5]\cdot O^{\cdot}\}^{2-} \xrightarrow{\text{fast}} 1/2\ \{[L^nCo^{III}NCFe^{II}(CN)_5]\cdot O\}_2^{4-} \quad \textbf{(3.4)}$$

$$1/2\ \{[L^nCo^{III}NCFe^{II}(CN)_5]\cdot O\}_2^{4-} \xrightarrow{\text{fast}} [L^nCo^{III}NCFe^{II}(CN)_5]^- + 1/2\ O_2^{2-} \quad \textbf{(3.5)}$$

$$1/2\ O_2^{2-} + H_2O \underset{}{\overset{K_{a'}^{-1}}{\rightleftharpoons}} 1/2\ O_2H^- + OH^- \quad \textbf{(3.6)}$$

$$k_{obs} = \frac{K_{add}K_{dep}k_{et}[OH^-]^2}{1 + K_{add}[OH^-] + K_{add}K_{dep}[OH^-]^2} \quad \textbf{(3.7)}$$

and characterized for similar systems)[18,36,37] and outer-sphere reduction of the complex by another OH^- ion occurs in processes 2.2 and 2.3. Although the high oxidative power of the $^{\bullet}OH$ radical seems an impediment for such a mechanism under the pH conditions used, this radical deprotonates producing $O^{\bullet -}$ (2.4), which is a weaker oxidant,[47−49] and rapidly dimerizes to produce the final peroxo species, (2.5) and (2.6).[50] Even so, the plausible and unobserved oxidation of any of the C−H bonds present in the ligand by this $O^{\bullet -}$ radical represents an important reason for dismissing such a mechanism.

The inner-sphere process depicted in Scheme 3 represents a better approach, given the absence of the CH-reactive $O^{\bullet -}$ radical. The kinetics observed is also very well described by this reaction scheme, provided K_{dep} is very small (as expected), making the term $(K_{add}\times K_{dep})\times[OH^-]^2$ in eq 3.7 negligible. In this reaction scheme, the rate law term (a/b) corresponds to the second-order rate constant for the inner-sphere electron-transfer process, $K_{dep}\times k_{et}$, while b is, again, the adduct equilibrium formation constant K_{add}. This fact is still in perfect agreement with the thermal and pressure behavior obtained for the terms (a/b) and b explained before, which indicated the rate and equilibrium constant nature of the two terms, respectively. The expected increased acidity of the coordinated OH^- permits a further minimal deprotonation with a second OH^- ion.[19] The oxo-adduct produced reduces the Fe^{III} center via an inner-sphere reaction (3.3) giving a mixed-valence $\{Co^{III}/Fe^{II}\};O^{\bullet -}$ adduct. In this sequence, the reduced adduct undergoes dimerization (3.4) to produce a peroxo-bridged adduct that finally dissociates giving the peroxo species detected in the reaction mixture.

The values of the first- or second-order electron-transfer rate constant determined for the reduction of the set of $Co^{III}/$

(47) Hickel, B.; Sehested, K. *J. Phys. Chem.* **1991**, *95*, 744−747.
(48) Wander, R.; Gall, B. L.; Dorfman, L. M. *J. Phys. Chem.* **1970**, *74*, 1819−1821.
(49) Simic, M.; Hoffman, M. Z.; Ebert, M. *J. Phys. Chem.* **1973**, *77*, 1117−1120.
(50) Autrey, T.; Brown, A. K.; Camaioni, D. M.; Dupuis, M.; Foster, N. S.; Getty, A. *J. Am. Chem. Soc.* **2004**, *126*, 3680−3681.

Fe^{III} complexes, depicted in Table 3, show the opposite trend than that expected from the value of $E°$ alone. The Fe^{III}/Fe^{II} redox potentials do not vary significantly: 612, 626, 644, and 649 mV for *trans*-$[L^{15}Co^{III}NCFe^{III}(CN)_5]$, *cis*-$[L^{13}Co^{III}NCFe^{III}(CN)_5]$, *trans*-$[L^{14}Co^{III}NCFe^{III}(CN)_5]$, and *trans*-$[L^{14S}Co^{III}NCFe^{III}(CN)_5]$ complexes.[15,16] While the values of the electron-transfer rate constant for *trans*-$[L^{14}Co^{III}NCFe^{III}(CN)_5]$ and *trans*-$[L^{14S}Co^{III}NCFe^{III}(CN)_5]$ are very similar and correspond to the slowest processes, for the *trans*-$[L^{15}Co^{III}NCFe^{III}(CN)_5]$ complex the value is 2 orders of magnitude larger and for *trans*-$[L^{13}Co^{III}NCFe^{III}(CN)_5]$ the value is in the middle. It is clear then that the rate variations do not point to ground state differences, $\Delta G°$ not being definitive for the kinetics observed. The determined $\Delta H^{‡}$ values are extraordinarily small in all cases, and they account for the readiness of the reduction reaction, especially for the L^{15} complex. Similar small $\Delta H^{‡}$ values have been determined for other reduction processes of Fe^{III} complexes with ascorbic acid.[51] The values of $\Delta S^{‡}$ are clearly negative and large, corresponding to a highly ordered transition state, accompanied by a small contraction as seen by the volume of activation. For the complex *trans*-$[L^{14S}Co^{III}NCFe^{III}(CN)_5]$, the value of $\Delta H^{‡}$ is larger while $\Delta S^{‡}$ is less negative than $\Delta V^{‡}$.

In contrast to the oxidation processes in the previous section, there is a correlation between the values of $\Delta S^{‡}$ and $\Delta V^{‡}$, indicating that no important solvent-assisted hydrogen bonding interactions are occurring on the transition state. This correlation further favors Scheme 3 vs Scheme 2, as it does not agree with the important differences expected in the signs of the ordering and compression parameters.[15,52,53] The small values of $\Delta H^{‡}$ also agree with the operation of the latter reaction mechanism proposed; the value of $\Delta H°$ for K_{dep} is expected to be very small indicating that the actual electron-transfer process (3.3) is not enthalpy demanding, as expected. As for the values of $\Delta S^{‡}$ and $\Delta V^{‡}$, they should include the values for the equilibrium depicted by K_{dep}, which are also expected to be small given the fact that no charges are created or neutralized during the process. Finally, although very noticeable, the above-mentioned important disagreement between the $\Delta G°$ and the facile nature of the reduction reaction supports the reaction mechanism proposed. The process does not correspond with an electron transfer between the OH^- ion and the Co^{III}/Fe^{III} complex.

The values of K_{add} that correspond to the term *b* in Table 3 are the same within the experimental error for all the systems. The value is independent of the $\{L^nCo\}$ unit of the dinuclear complex; this moiety does not play an important role in its magnitude. Although this similarity could indicate that the OH^- adduct is formed on one of the nonbridging cyanide groups, the electronic distribution of the bridging cyanide ligand makes it more susceptible to attack at the cyanide carbon. The fact that differences on K_{add} are expected to be small and the kinetic methodology used is not ideal[54] makes any further comments on the agreement between these values tenuous. Any attempts to spectrophotometrically detect this adduct have been unsuccessful, given the very rapid reduction reaction. The detection of equivalent adducts from the reduced Co^{III}/Fe^{II} form also proved fruitless; the lower charge on the iron center probably disfavors the formation of such a species even more so. In this respect, we have been pursuing the inclusion of mixed-valence Co^{III}/Fe^{II} complexes in silica matrixes;[55] the IR and ^{13}C NMR signals of cyanides in these solids are displaced to the C═N zone in both cases, despite the fact that the reversible redox process observed corresponds to the original cyanide-bridged complexes. Similar interactions to that observed in this case of the C≡N bond with the −OR groups of the silica matrix can be held responsible for this difference.

Conclusions. The recent preparation of the mixed-valence complex *trans*-$[L^{14S}Co^{III}NCFe^{II}(CN)_5]^-$ has allowed for a full comparison of outer-sphere oxidation processes with related N_5 donor complexes, indicating that the reaction involves a high degree of solvent-assisted hydrogen bonding that clearly differentiates between N_5 and N_3S_2 coordinated cobalt(III) complexes. The oxidation reaction to the Co^{III}/Fe^{III} complexes is found to be reversible at high pH producing the original mixed-valence complexes and hydrogen peroxide. The reaction is found to have a second-order dependence on $[OH^-]$ indicating the preliminary formation and deprotonation of an OH^- adduct that undergoes a inner-sphere redox process. The pressure and thermal activation parameters, and their correlations, indicate that the reaction is enthalpy driven and they agree with the proposed inner-sphere character.

Acknowledgment. We acknowledge financial support for the ACI2003-17, BQU2001-3205, and A10027090 projects from the DURSI, Ministerio de Ciencia y Tecnología, and Australian Research Council; we also thank PEDECIBA-Química for financial help.

Supporting Information Available: Crystallographic data in CIF format; values of k_{obs} for the oxidation of *trans*-$[L^{14S}Co^{III}NCFe^{II}(CN)_5]^-$ as a function of the oxidizing agent, pH, temperature, pressure, and oxidizing agent concentration; values determined for k_{obs} for the reduction reaction determined as a function of the dinuclear complex, $[OH^-]$, temperature, and pressure; plots of the dependence of the value of k_{obs} on the concentration of oxidizing agent for the reactions of *trans*-$[L^{14S}Co^{III}NCFe^{II}(CN)_5]^-$ with $S_2O_8^{2-}$ and $[Co(ox)_3]^{3-}$. This material is available free of charge via the Internet at http://pubs.acs.org.

IC0493191

(51) Chaterjee, D. *Polyhedron* **1999**, *18*, 1767−1771.
(52) Benzo, F.; Bernhardt, P. V.; González, G.; Martínez, M. *J. Chem. Soc., Dalton Trans.* **1999**, 3973−3979.
(53) Bernhardt, P. V.; Gallego, C.; Martínez, M.; Parella, T. *Inorg. Chem.* **2002**, *41*, 1747−1754.
(54) Ooi, B.; Sykes, A. G. *Inorg. Chem.* **1988**, *27*, 310−315.
(55) García-Basallote, M.; Martínez, M. Unpublished results.